Supplemental Material and Methods

Nr4a1^{KO} and wild type littermate animal studies were conducted at Brigham Young University and followed all NIH animal welfare guidelines. Generation of the *Nr4a1*^{KO} mice was previously described (1). Mice were sacrificed at 8-12 weeks of age. Pancreatic islets were isolated from *Nr4a1*^{KO} and wild type littermate mice using a collagenase digestion procedure as previously described (2), after which islets were hand-picked to remove contaminating acinar tissue.

Foxp^{TKO} and wild type littermate animal studies were conducted at the University of Wisconsin-Madison and followed all NIH animal welfare guidelines. Generation of *Foxp*^{TKO} mice was previously described (3). Mice were sacrificed at 12-14 weeks of age. Pancreatic islets were isolated from *Foxp*^{TKO} and wild type littermate mice using a collagenase digestion procedure as previously described (2), after which islets were hand-picked to remove contaminating acinar tissue.

Adenoviral transduction

As described previously (4), constitutively active forms of mouse *Nfatc1* and *Nfatc2* were overexpressed in human islets with high-titer purified adenoviruses (Vector Biolabs, Malvern, PA); GFP or LacZ were used as negative controls (4). All genes were expressed under the control of the cytomegalovirus (CMV) promoter, and thus, did not yield cell type-specific expression. Briefly, human islets were incubated for 3 minutes at 37˚C in magnesium and calcium-free HBSS medium (Gibco) containing 2 mM EGTA, as we have found this procedure to improve the efficiency and coverage of adenoviral-mediated gene expression. Islets were then transduced with the adenoviruses at an MOI of 200 in 200 µL of islet transduction media (RPMI 1640 supplemented with 8.0 mM glucose, 1% antibiotic-antimycotic (Gibco), and 5 mM HEPES) for 15 minutes at 37˚C. After transduction, Islets were transferred to sterile non-TC treated 60 mm dish containing 3.5 mL of the transduction media and incubated in a humidified 5% CO_2 incubator overnight at 37˚C. The following day, islets were placed into 4 mL of Human islet culture media containing

RPMI 1640 supplemented with 8.0 mM glucose, 1% antibiotic/antimycotic, 5 mM HEPES, and 10% FBS. Islets were harvested 48 hours after adenoviral transduction and were assessed by cellular proliferation assays, RNA-seq, ChIP-seq, or ATAC-seq.

Cellular proliferation measures in mouse islets

Measurement of NFATC2-induced cellular proliferation in wild type, *Nr4a1*^{KO} and *Foxp*^{TKO} mice was carried out as described previously (4). Briefly, following collagenase-digestion of the pancreas, acinar-free islets were hand-picked, washed twice in islet media (RPMI 1640 with 8 mM glucose, 10% fetal bovine serum, 1% penicillin/streptomycin), and separated into groups of 200 islets/condition. Islets were then left untreated or transduced with Ad-GFP or Ad-ca-Nfatc2 at a MOI of ~200 for 24 hours, as previously described (2, 4). [^{3}H-methyl]-thymidine (1 mCi/ml, Perkin Elmer) was added at a final concentration of 1 μCi/mL to groups of ~200 islets for the final 24 hours of culture (4). Groups of 50 islets were picked in triplicate, washed twice in RPMI-1640 with unlabeled thymidine, twice in PBS, and then the DNA was precipitated with 500 μL of cold 10% trichloroacetic acid and solubilized with addition of 100 μL of 0.3 N NaOH (2, 5, 6). [^{3}H]-thymidine incorporation was measured by liquid scintillation counting and normalized to total cellular protein, as measured by Bradford assay.

NFATC2 ChIP-seq in human islets

48 hours after Ad-ca-Nfatc2 treatment, ~17,000 human IEQs were incubated with 5 mL of 1% formaldehyde (Thermo Scientific, 28906) in PBS for 5 minutes at room temperature. To quench the formaldehyde fixative, 256 μL of 2.5 mM glycine was added, incubated for 2 minutes, and then centrifuged (500 x g) to pellet the islets. Islets were washed with 1mL each of PBS, NCP buffer 1 (10 mM HEPES pH 6.5, 10 mM EDTA, 0.5 mM EGTA, 0.25% Triton X-100) and NCP buffer 2 (200 mM NaCl, 10 mM HEPES pH 6.5, 1 mM EDTA, 0.5 mM EGTA). Islets were then lysed in 3 mL of lysis buffer (50 mM Tris-HCl pH 8.0, 10 mM EDTA, 0.5% Empigen BB, 1% SDS, 1mM PMSF, and Roche cOmplete Mini EDTA-free Protease Inhibitor Cocktail Tablet). The islets were triturated with a 30-gauge needle ~20 times, and then sonicated using a Branson Digital

Sonifier 250 with a double step microtip probe at 30% amplitude for 15 cycles (30 seconds on, 30 seconds off). The sample was then centrifuged (13000 x g, 10 minutes, 4˚C), and supernatant collected for immunoprecipitation. The supernatant was diluted with IP buffer (20 mM Tris-HCl pH 8.0, 2 mM EDTA, 150 mM NaCl, 1% Triton X-100) at a ratio 5:2, IP buffer:supernatant; 10% of the supernatant was set aside for ChIP input determination. To the IP buffer/supernatant mixture, 10 µL of anti-HA antibody (Abcam, ab9110) was used to immunoprecipitate HA-tagged NFATC2/chromatin complexes overnight at 4˚C. The following day 100 µL Protein A/G magnetic beads (Pierce) were supplied to the immunoprecipitated mixture for 2 hours. The magnetic bead complexes were then sequentially washed with 1 mL of wash buffer #1 (2 mM EDTA, 20 mM Tris-HCl pH 8.0, 0.1% SDS, 1% Triton X-100, 150 mM NaCl), wash buffer #2 (2 mM EDTA, 20 mM Tris-HCl pH 8.0, 0.1% SDS, 1% Triton X-100, 500 mM NaCl), and wash buffer #3 (1 mM EDTA, 10 mM Tris-HCl pH 8.0, 250 mM LiCl, 1% sodium deoxycholate, 1% NP-40 Alternative), followed by 5 washes in TE buffer. The NFATC2/chromatin complexes were then eluted with elution buffer (200 mM NaCl, 100 mM NaHCO3, and 1% SDS) at 65˚C overnight. Eluted DNA was purified using MinElute PCR purification cleanup kit (Qiagen).

All sequencing studies were performed at the University of Wisconsin-Madison Biotechnology Center. DNA concentration and size distribution were verified using the Qubit dsDNA HS Assay Kit (Invitrogen, Carlsbad, California, USA) and Agilent DNA HS chip (Agilent Technologies, Inc., Santa Clara, CA, USA), respectively. Samples were prepared according the TruSeq ChIP Sample Preparation kit (Illumina Inc., San Diego, California, USA) with minor modifications. Libraries were size-selected for an average insert size of 350 bp using SPRI-based bead selection. Quality and quantity of the finished libraries were assessed using an Agilent DNA1000 chip and Qubit dsDNA HS Assay Kit, respectively. Libraries were standardized to 2 nM. Paired end 125bp sequencing was performed to a depth of 68 – 154 million reads per sample, using SBS chemistry (v4) on an Illumina HiSeq2500. Images were analyzed using the standard Illumina Pipeline, version 1.8.2.

The raw reads from all samples were aligned to human reference genome (hg19) with Bowtie 2 (version 2.3.1). We used Bowtie2 default reporting mode with the argument *-X 550 --no-mixed --no-discordant* being specified. Picard MarkDuplicates tool (version 2.9.2) was used to remove duplicate reads from the alignment. We performed peak calling from mapped and properly paired reads with Bioconductor package MOSAiCS (version 3.5). The peak sets called from the six samples were merged and 8,635 peaks were retained based on the following criteria. We included (i) peaks reproducible in at least two samples and (ii) peaks identified in one sample, whose summit signals are higher than the third quantile of the summit signals of the reproducible peaks. Further, peaks in ENCODE DAC blacklist regions were dropped from the peak list.

De novo motif analysis was performed using MEME-ChIP and identified TTTCCR as the most significant motif present at all NFATC2 binding sites. This motif is similar to a known NFATC2 motif with a Fisher's exact test p-value = $2.0e^{-668}$ (7). To identify motifs that co-occur at NFATC2 binding sites, we performed spaced motif analysis (SPAMO) on the sequences around the summits of the merged peaks (8). We discovered the FOXP1 motif, MA0481.2, significantly co-occurred with the NFATC2 motif (E-score of 0.0022). We used FIMO to confirm the co-occurrence of NFATC2 and FOXP1 motifs, and to compute the binding proximity (9). Co-occurrence from the dependency between NFATC2 and FOXP1 motif occurrences that Pearson's chi-square testing supports with p-value less than $2.2e^{-16}$. The partner TFs may bind to DNA sequences of the 4,349 peaks where the both motifs are identified, within a window of 500 bp at most, having 26.9% of them sharing binding sites (1170/4349).

The ChIPseeker R package (v1.14.2) was used to annotate peaks and their transcriptional start sites (TSS) within 3kb (10). The annotatePeak function annotated regions in priority order: promoters, 5' and 3' UTRs, exons, introns, downstream, and intergenic regions. The reference database for annotation used was set to annoDb=org.Hs.eg.db.

Sequencing of human islet transcriptome

48 hours after adenoviral treatment, ~6,000 human IEQs per condition (Ad-GFP, Ad-ca-Nfatc1 and Ad-ca-Nfatc2), islets were collected, and washed twice with ice-cold PBS. The human islets were lysed with 350 µL of QIAzol Lysis Reagent (Qiagen) and stored at -80˚C before purifying RNA using Mini RNeasy purification kits per manufacturer's instructions.

Total RNA submitted to the University of Wisconsin-Madison Biotechnology Center was verified for purity and integrity via the NanoDrop2000 Spectrophotometer and Agilent 2100 BioAnalyzer, respectively. Samples that met the Illumina sample input guidelines were prepared according the TruSeq Stranded Total RNA Sample Preparation Guide (Rev. E) using the Illumina TruSeq Stranded Total RNA Sample Prep Gold kit (Illumina Inc., San Diego, California, USA) as directed. For each library preparation, 1ug of total RNA was ribosomally reduced and purified by paramagnetic beads (Agencourt RNA Clean XP beads, Beckman Coulter, Indianapolis IN, USA). Subsequently, each rRNA depleted sample was fragmented using divalent cations under elevated temperature. The fragmented RNA was synthesized into double-stranded cDNA using SuperScript II Reverse Transcriptase (Invitrogen, Carlsbad, California, USA) and random primers for first strand cDNA synthesis followed by second strand synthesis using DNA Polymerase I and RNase H for removal of mRNA. Double-stranded cDNA was purified by paramagnetic beads (Agencourt AMPure XP beads, Beckman Coulter). The cDNA products were incubated with Klenow DNA Polymerase to add an 'A' base (Adenine) to the 3' end of the blunt DNA fragments. DNA fragments were ligated to Illumina adapters, which have a single 'T' base (Thymine) overhang at their 3'end. The adapter-ligated DNA products were purified by paramagnetic beads. Adapter ligated DNA was amplified in a Linker Mediated PCR reaction (LM-PCR) for 10 cycles using Phusion DNA Polymerase and Illumina's PE genomic DNA primer set and then purified by paramagnetic beads. Quality and quantity of the finished libraries were assessed using the AATI Fragment Analyzer (Agilent Technologies, Inc., Santa Clara, CA, USA) and BioPlex Synergy 2 Plate Reader (BioTek Instruments, Winooski, VT, USA), respectively. Libraries were standardized to 2nM. Cluster generation was performed using the Illumina cBot. Single end 100bp sequencing

was performed to a depth of 31 – 46 million reads, using v4 SBS chemistry on an Illumina HiSeq2500 sequencer. Images were analyzed using the standard Illumina Pipeline, version 1.8.2.

The human islet RNA-sequencing reads were mapped via bowtie against the refseq hg19 reference (11). Gene expression values were then estimated via RSEM (12). Expected counts were normalized using median-by-ratio normalization (13). EB-seq was used to classify genes into 5 distinct patterns of differential expression (14). For each gene, EB-seq computed a posterior probability (PP) associated with each expression pattern. The higher the PP for a particular pattern, the more likely the gene is following that pattern. Differential expression (DE) was defined by between the three conditions: (GFP-Control, C1-NFATC1, and C2-NFATC2). Pattern 1: C1 = C2 = GFP (no DE); Pattern 2: C1 = C2 ≠ GFP (DE for C1 and C2 equally); Pattern 3: C2 ≠ C1 = GFP (DE for C2 only); Pattern 4: C1 ≠ C2 = GFP (DE for C1 only); and Pattern 5: C1 ≠ C2 ≠ GFP (DE for C1 and C2 unequally). **Table S14** contains RSEM-normalized expression values, as well as the PP values for patterns 1–5 for all genes. We identified genes as DE in a particular pattern (PP1-PP5) as those with posterior probability of Pattern 1 < 0.05 and the maximum posterior probability value. Human-mouse ortholog genes were annotated using biomaRt (v2.33.4). **Table S15** contains all human and mouse ortholog genes with expression measured in mouse and human islets. All statistical analyses were carried out using R version 3.4.1.

To estimate the magnitude of expression for ca-Nfatc1 and ca-Nfatc2 in human islets, we computed their mean expression values for islets transduced with Ad-ca-Nfatc1, Ad-ca-Nfatc2, or Ad-GFP. Exogenous ca-Nfatc1 and ca-Nfatc2 transcripts were distinguished from endogenous NFATC1 and NFATC2 transcripts by using modified reference transcriptomes. The expression of ca-Nfatc1 and ca-Nfatc2 was ~900 and ~200-fold greater than endogenous NFATC1 and NFATC2 expression, respectively.

ATAC-seq sample preparation

48 hours after GFP or ca-Nfatc2 adenoviral transduction, 50 average sized human islets were picked into a 1.7 mL tube. The islets were washed with 500 µL of PBS at 4˚C and pelleted by

centrifugation at 100 x g for 1 minute. 300 µL of ATAC Lysis buffer (10 mM Tris-HCl pH 7.4, 10 mM NaCl, 3 mM MgCl2, 0.1% IGEPAL CA-630) was used to resuspend the islets. The islets were incubated for 20 minutes on ice. After incubating, the islets were lysed by trituration with a 25 gauge needle essentially until intact islets were no longer visible. The lysate was centrifuged at 500 x g for 10 minutes at 4˚C. This generated a crude nuclei pellet and a supernatant. The supernatant was discarded and the nuclei pellet was washed with 100 µL of ATAC Lysis buffer in order to reduce cytoplasm and mitochondrial contamination. This mixture was centrifuged at 500 x g for 10 minutes at 4˚C and the supernatant was removed. Per ATAC-seq sample, a mixture of 25 µL 2x TDE buffer, 22.5 µL nuclease-free water, and 2.5 µL TDE1 transposase enzyme (Nextera DNA Library Prep kit, Illumina) was applied and incubated for 30 minutes in a 37˚C water bath. The samples were then purified using a MinElute Reaction cleanup kit (Qiagen) and eluted using two sequential aliquots of 10 µL EB buffer. After purification all ATAC samples were kept at -80˚C. All ATAC-seq samples were transposed and frozen prior to preparing all libraries. Libraries were amplified using 20 µL of ATAC sample, 10 µL of unique dual indexes (IDT for Illumina Nextera DNA UD Indexes Set A (96 Indexes, 96 Samples)), and 30 µL of NEBNext High Fidelity 2 x PCR Master Mix. Each ATAC sample was amplified by 12 cycles which was determined by qPCR to be saturating for the libraries. The PCR thermocycler was set to 72˚C for 5 minutes, 98˚C for 30 seconds, and then 12 total cycles of 98˚C for 10 seconds, 63˚C for 30 seconds, 72˚C for 1 minute. After amplification the libraries were purified using MinElute PCR purification cleanup kit (Qiagen). The libraries were sequenced to a depth of 104-182 million reads using paired-end 150 bp reads on a NovaSeq 6000 (Illumina) at the University of Wisconsin Biotechnology Center DNA Sequencing Facility.

ATAC-seq data analysis

Illumina Nextera adapters were trimmed with cutadapt (version 2.0) with option “-q 30 --minimum-length 36”. Paired-end ATAC-seq reads were aligned to the human genome assembly (hg19) with bowtie2 (version 2.3.4.1) with option “-X 800 --no-mixed --no-discordant” (15). For

each sample, unmapped reads were filtered out by using SAMtools view (version 1.8) (16), with option “-F 4” and mitochondrial reads were removed. Duplicate reads were removed with Picard tools (version 2.9.2). We obtained on average 105 ± 20 million reads per sample.

In total, 231,232 master ATAC peaks (mean width 663 ± 393 bp) were called for pooled GFP and NFATC2 samples with MACS2 (17). We utilized “getCounts()” function in chromVAR (18) to obtain the count matrix of Tn5 cuts. We then performed differential accessibility analysis with DESeq2 (19) and obtained NFATC2 opening and closing chromatin. The genomic compartment annotations were obtained using ChIPseeker (10). Motif enrichment analysis was performed using with MEME-CHIP (7).

Noncoding RNA-seq library preparation

Total RNA was extracted by QIAzol Lysis Reagent (Qiagen), followed by ribosomal and polyA depletion. After RiboZero purification and oligo-dT depletion, RNA Barcoded Libraries were prepared according to Illumina's instructions (2013) accompanying the TruSeq RNA Sample prep kit v2 (Part# RS-122-2001). Libraries were quantified using the Agilent Bioanalyzer (model 2100) and pooled in equimolar amounts. The pooled libraries were sequenced with 100-bp paired-end reads on the HiSeq 4000 in Rapid Run Mode following the manufacturer's protocols (2013).

Noncoding RNA-Seq Data analysis

Non-coding RNA-seq data analysis was performed as described in Perez-Cervantes and Smith et al. 2020 (20). Briefly, Fastq files were aligned to UCSC genome build hg19 using STAR (v2.5.1), transcript assembly was performed by Stringtie (version 1.3.3) and merged with the Stringtie ‘merge’ function. Counts were retrieved from the merged transcriptome with HTseq (v0.6) differential expression was performed with R (3.4) package DEseq2 (19). False discovery rate (FDR) was calculated after removing the coding-gene transcripts, ncRNA that overlapped coding genes in the same strand (bedtools intersect 2.29.0), and RNAs shorter than 100 base pairs. Transcripts associated with miRNA, tRNA, and rRNA are not included in the ncRNA analysis. Significance was considered to have been reached when FDR was <0.05 and $|\log_2$ fold-

change| was >0.5. Open chromatin peaks and TF-binding peaks were intersected with ncRNAs using Bioconductor package GenomicRanges (21) allowing for a 1000 bp gap upstream the 5' end of the RNA and 50 bp into the RNA. These data can be visualized in the UCSC genome browser here:

http://genome.ucsc.edu/s/ssimonett/hg19_Nfatc2_human_islet_genome_browser.

Coimmunoprecipitation

Human-derived EndoC-βH2 (22) β-cells were transduced in a 6 well plate with either Ad-GFP or Ad-ca-Nfatc2 (MOI 10, 24 hours). 48 hours after transduction, the cells were harvested, washed with PBS, and frozen at -80C. Lysis was performed using 100 µL of NET-seq lysis buffer (23) with protease inhibitors (Roche Protease Inhibitor Cocktail). Before removing cell debris, DNase I (10 Kunitz units, Qiagen) was added to the lysate and incubated at room temperature for 1 hour to digest larger DNA fragments. Following DNase, the lysate was centrifugation at 1000 x g for 2 mins. Protein concentration was measured by BCA, and equal amounts used for immunoprecipitation (40 µg); 4 µg total protein was used as the input control. Immunoprecipitation was performed by applying 2 µg of anti-HA antibody (ab9110) overnight with end over end rocking at 4˚C. 50 µL of protein A/G beads (Pierce, 88803) were equilibrated in the lysis buffer and applied to each sample for 2 hours with end over end rocking at room temperature. The beads were washed five times with 500 µL of NET-seq lysis buffer. Elution was performed using 30 µL of NET-seq lysis buffer and 12 µL of 2.5x SDS-PAGE loading dye while incubating at 95˚C for five minutes. The coimmunprecipitation was validated using Western blot and probed with a 1:2000 dilution of anti-FOXP4 antibody (Sigma, HPA007176).

EdU measurements

Measurement of NFATC2-induced cellular proliferation in wild type and *Nr4a1*^{KO} mice was modified from that previously described (24). Briefly, islets were treated for 48 hours with Ad-ca-Nfatc2, Ad-LacZ, or no virus control with 10 µM EdU daily media changes. After incubation, 50 islets were handpicked into eppendorf tubes, washed with PBS, and spun for 5 minutes at 900 x

g. Following centrifugation the supernatant was removed and 100 µL of 0.05% trypsin was added, and tubes were placed in 37ºC incubator for 5 mins with gentle mixing every minute. 1 mL of supplemented RPMI media was then added to each tube and samples were collected via centrifugation leaving 100 µL of liquid with pellet. Poly-D-lysine cover slips (EMS) were placed inside of sterile 12 well plates and 50 µL of media mixture was spotted on the middle of 2 cover slips. Plates were placed in 37ºC incubator for 6 hours to allow cells to adhere. EdU staining was then performed according to manufacturer's protocol (Invitrogen). After EdU detection, half of the coverslips were stained for insulin (Dako, A0564) and other half for glucagon (Sigma, G2654) and somatostatin (Santa Cruz, sc-7819). Five images per replicate were evaluated for EdU and insulin or glucagon and somatostatin signals for each condition.

Gene set enrichment

Allez was used to identify statistically enriched Gene Ontology (GO) categories in selected gene sets compared to random, same-sized gene sets. From these comparisons, adjusted p-values and Z-scores are tabulated (25).

References

1. Lee SL, Wesselschmidt RL, Linette GP, Kanagawa O, Russell JH, and Milbrandt J. Unimpaired thymic and peripheral T cell death in mice lacking the nuclear receptor NGFI-B (Nur77). *Science.* 1995;269(5223):532-5.
2. Tessem JS, Moss LG, Chao LC, Arlotto M, Lu DH, Jensen MV, et al. Nkx6.1 regulates islet beta-cell proliferation via Nr4a1 and Nr4a3 nuclear receptors. *Proceedings of the National Academy of Sciences of the United States of America.* 2014;111(14):5242-7.
3. Spaeth JM, Hunter CS, Bonatakis L, Guo M, French CA, Slack I, et al. The FOXP1, FOXP2 and FOXP4 transcription factors are required for islet alpha cell proliferation and function in mice. *Diabetologia.* 2015;58(8):1836-44.
4. Keller MP, Paul PK, Rabaglia ME, Stapleton DS, Schueler KL, Broman AT, et al. The Transcription Factor Nfatc2 Regulates beta-Cell Proliferation and Genes Associated with Type 2 Diabetes in Mouse and Human Islets. *PLoS genetics.* 2016;12(12):e1006466.
5. Ray JD, Kener KB, Bitner BF, Wright BJ, Ballard MS, Barrett EJ, et al. Nkx6.1-mediated insulin secretion and beta-cell proliferation is dependent on upregulation of c-Fos. *FEBS Lett.* 2016;590(12):1791-803.
6. Draney C, Austin MC, Leifer AH, Smith CJ, Kener KB, Aitken TJ, et al. HDAC1 overexpression enhances beta-cell proliferation by down-regulating Cdkn1b/p27. *The Biochemical journal.* 2018;475(24):3997-4010.
7. Machanick P, and Bailey TL. MEME-ChIP: motif analysis of large DNA datasets. *Bioinformatics.* 2011;27(12):1696-7.
8. Whitington T, Frith MC, Johnson J, and Bailey TL. Inferring transcription factor complexes from ChIP-seq data. *Nucleic acids research.* 2011;39(15):e98.
9. Grant CE, Bailey TL, and Noble WS. FIMO: scanning for occurrences of a given motif. *Bioinformatics.* 2011;27(7):1017-8.
10. Yu G, Wang LG, and He QY. ChIPseeker: an R/Bioconductor package for ChIP peak annotation, comparison and visualization. *Bioinformatics.* 2015;31(14):2382-3.
11. Langmead B, Trapnell C, Pop M, and Salzberg SL. Ultrafast and memory-efficient alignment of short DNA sequences to the human genome. *Genome Biol.* 2009;10(3):R25.
12. Li B, and Dewey CN. RSEM: accurate transcript quantification from RNA-Seq data with or without a reference genome. *BMC bioinformatics.* 2011;12:323.
13. Anders S, McCarthy DJ, Chen Y, Okoniewski M, Smyth GK, Huber W, et al. Count-based differential expression analysis of RNA sequencing data using R and Bioconductor. *Nat Protoc.* 2013;8(9):1765-86.
14. Leng N, Dawson JA, Thomson JA, Ruotti V, Rissman AI, Smits BM, et al. EBSeq: an empirical Bayes hierarchical model for inference in RNA-seq experiments. *Bioinformatics.* 2013;29(8):1035-43.
15. Langmead B, and Salzberg SL. Fast gapped-read alignment with Bowtie 2. *Nature methods.* 2012;9(4):357-9.
16. Li H, Handsaker B, Wysoker A, Fennell T, Ruan J, Homer N, et al. The Sequence Alignment/Map format and SAMtools. *Bioinformatics.* 2009;25(16):2078-9.
17. Zhang Y, Liu T, Meyer CA, Eeckhoute J, Johnson DS, Bernstein BE, et al. Model-based analysis of ChIP-Seq (MACS). *Genome Biol.* 2008;9(9):R137.
18. Schep AN, Wu B, Buenrostro JD, and Greenleaf WJ. chromVAR: inferring transcription-factor-associated accessibility from single-cell epigenomic data. *Nature methods.* 2017;14(10):975-8.
19. Love MI, Huber W, and Anders S. Moderated estimation of fold change and dispersion for RNA-seq data with DESeq2. *Genome Biol.* 2014;15(12):550.

20. Perez-Cervantes C, Smith LA, Nadadur RD, Hughes AEO, Wang S, Corbo JC, et al. Enhancer transcription identifies cis-regulatory elements for photoreceptor cell types. *Development.* 2020;147(3).
21. Lawrence M, Huber W, Pages H, Aboyoun P, Carlson M, Gentleman R, et al. Software for computing and annotating genomic ranges. *PLoS Comput Biol.* 2013;9(8):e1003118.
22. Scharfmann R, Pechberty S, Hazhouz Y, von Bulow M, Bricout-Neveu E, Grenier-Godard M, et al. Development of a conditionally immortalized human pancreatic beta cell line. *J Clin Invest.* 2014;124(5):2087-98.
23. Churchman LS, and Weissman JS. Native elongating transcript sequencing (NET-seq). *Curr Protoc Mol Biol.* 2012;Chapter 4:Unit 4 14 1-7.
24. Tessem JS, Moss LG, Chao LC, Arlotto M, Lu D, Jensen MV, et al. Nkx6.1 regulates islet beta-cell proliferation via Nr4a1 and Nr4a3 nuclear receptors. *Proc Natl Acad Sci U S A.* 2014;111(14):5242-7.
25. Newton MA, Quintana FA, Den Boon JA, Sengupta S, and Ahlquist P. Random-Set Methods Identify Distinct Aspects of the Enrichment Signal in Gene-Set Analysis. *Annals of Applied Statistics.* 2007;1(1):85-106.

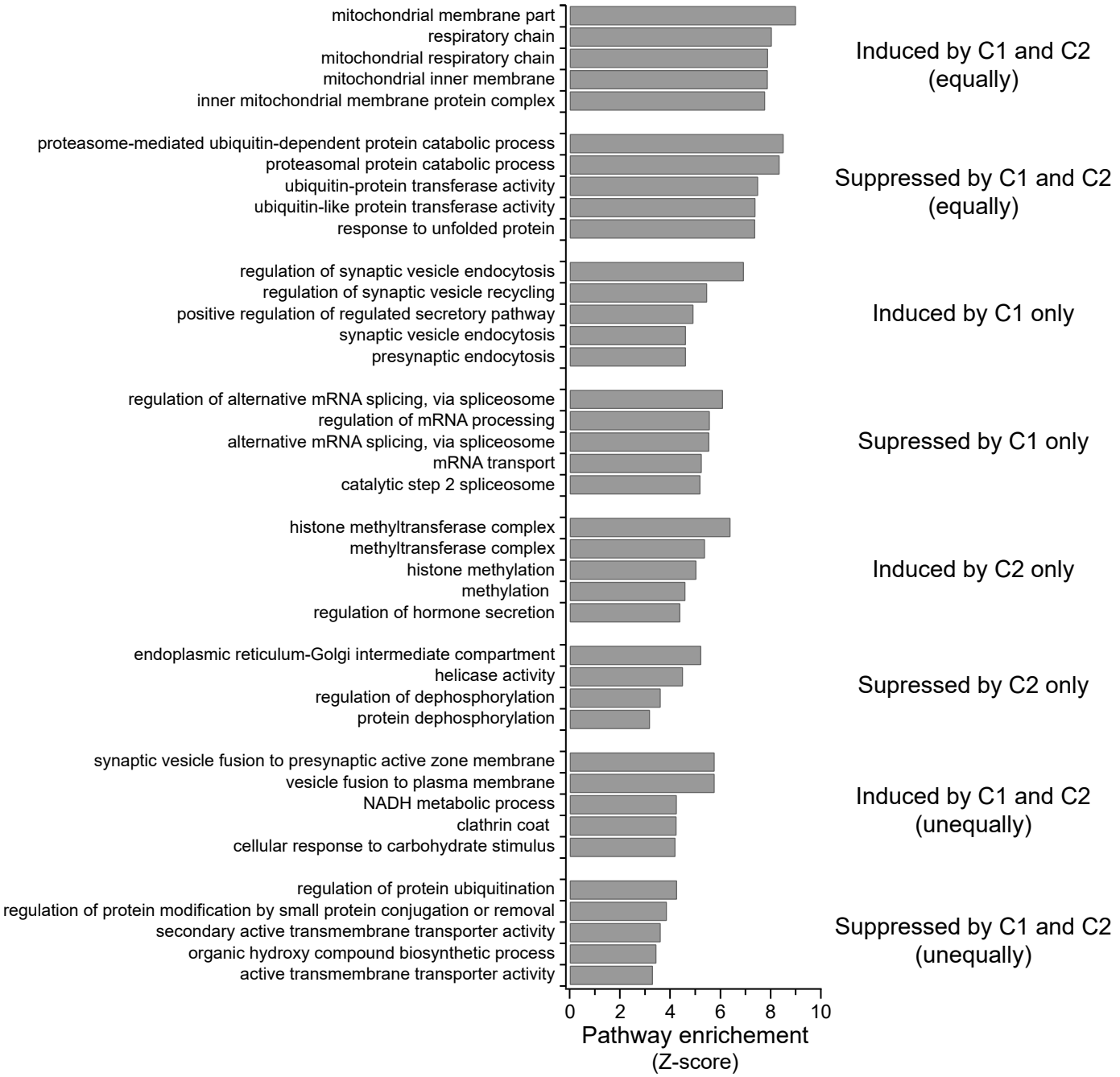

Figure S1. Gene set enrichment for all NFATC1 and NFATC2-regulated transcripts in human islets.

Whole islet RNA was quantified and classified using posterior probability into four differential expression patterns shown in Figure 1C-F. These genes sets were further sorted by direction of expression change indicated to the right of the plot. Pathway enrichment using ALLEZ was performed on these gene sets and shown as a Z-score. Only the top enriched terms are shown. All other terms can be found in Table S3.

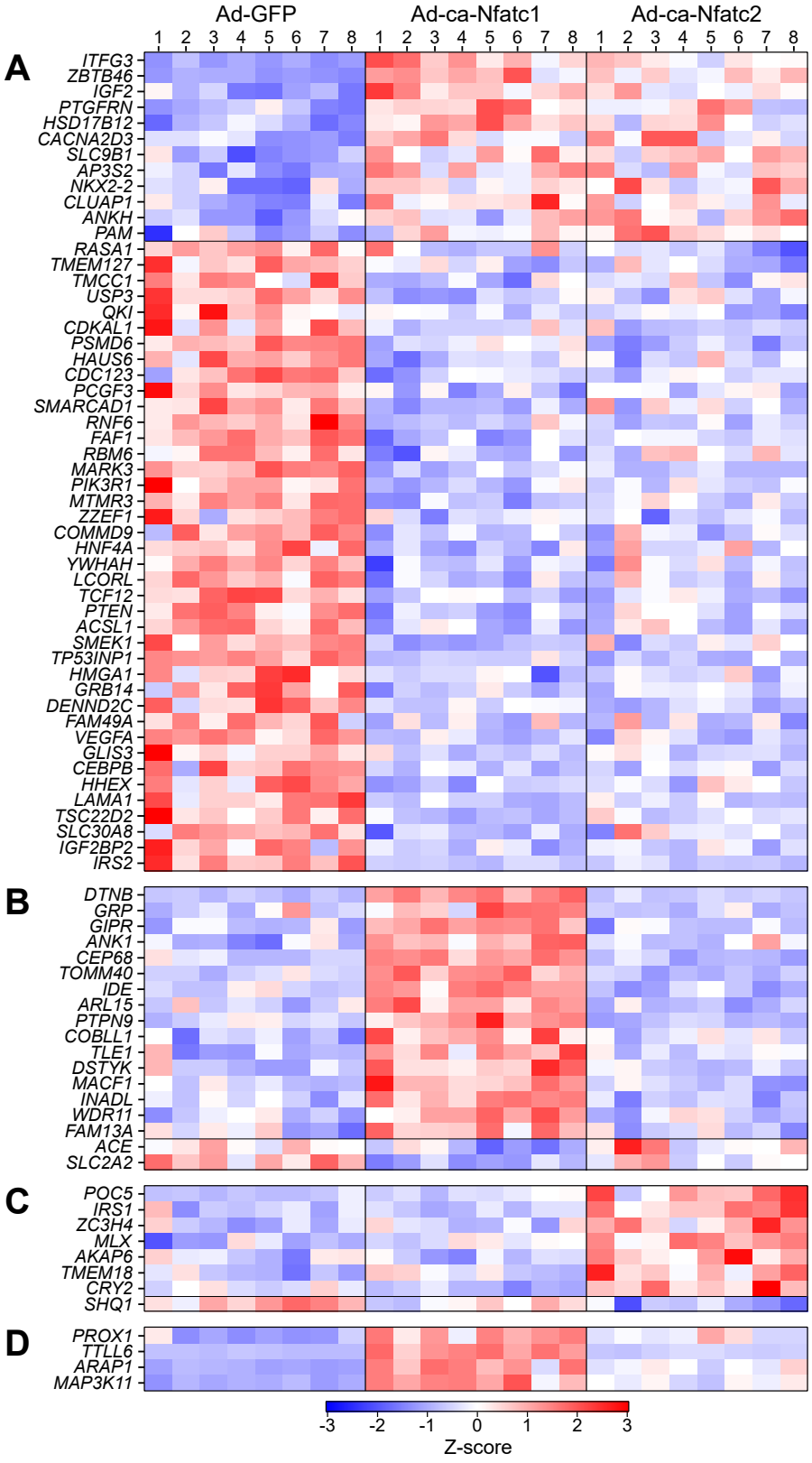

Figure S2. NFATC1 and NFATC2 regulate genes associated with diabetes in human GWAS. The expression of 82 out of 242 genes associated with diabetes in human GWAS were differentially regulated by NFATC1 and/or NFATC2 in human islets. Heat map illustrates the expression profiles for the 82 genes among 8 different human islet preparations, numbered 1 – 8, each having received either Ad-GFP (control), Ad-ca-Nfatc1 or Ad-ca-Nfatc2. Genes were grouped according to whether they were equally regulated by ca-Nfatc1 and ca-Nfatc2 A), regulated by ca-Nfatc1 only B), regulated by ca-Nfatc2 only C), or regulated by both NFAT isoforms, but to different magnitudes D). Gene expression values are shown as Z-scores; red corresponds to increased expression, blue corresponds to decreased expression.

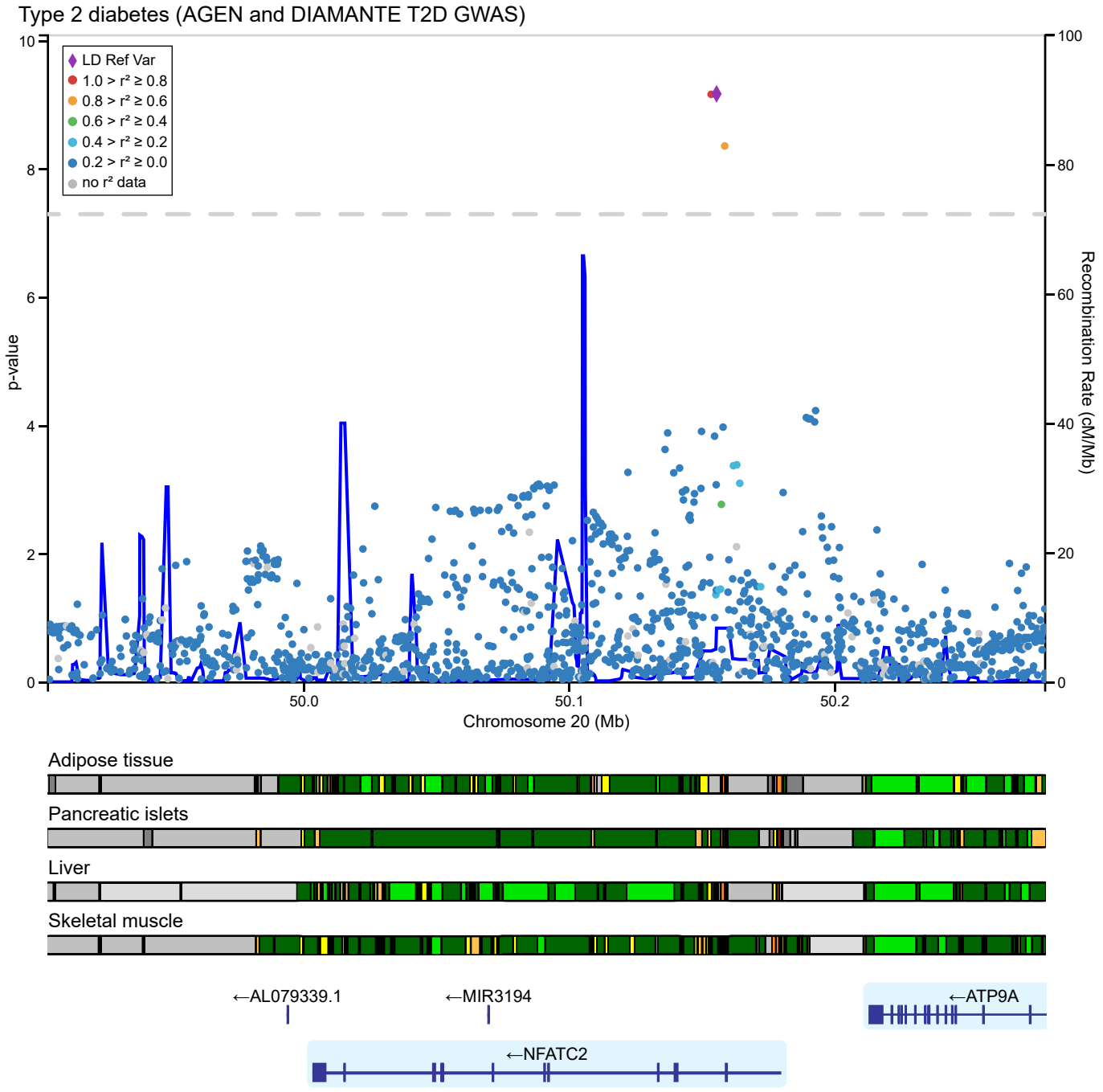

Figure S3. T2D regional association plot at *NFATC2* locus in human GWAS.
A regional association plot demonstrating the link between Type 2 Diabetes susceptibility and the *NFATC2* locus in humans. Each point is a nucleotide variant with an associated p-value demon-strated by the left y-axis. The lead variant is marked with a purple diamond and LD correlation of nearby SNPs is color coded according to the legend. Recombination frequency is graphed as a blue line in accordance with the right y-axis. Plot was generated using LocusZoom embedded in the AMP-T2DKP portal. Below the LocusZoom plot are tissue-specific chromatin state maps as described by Parker et. al. (44).

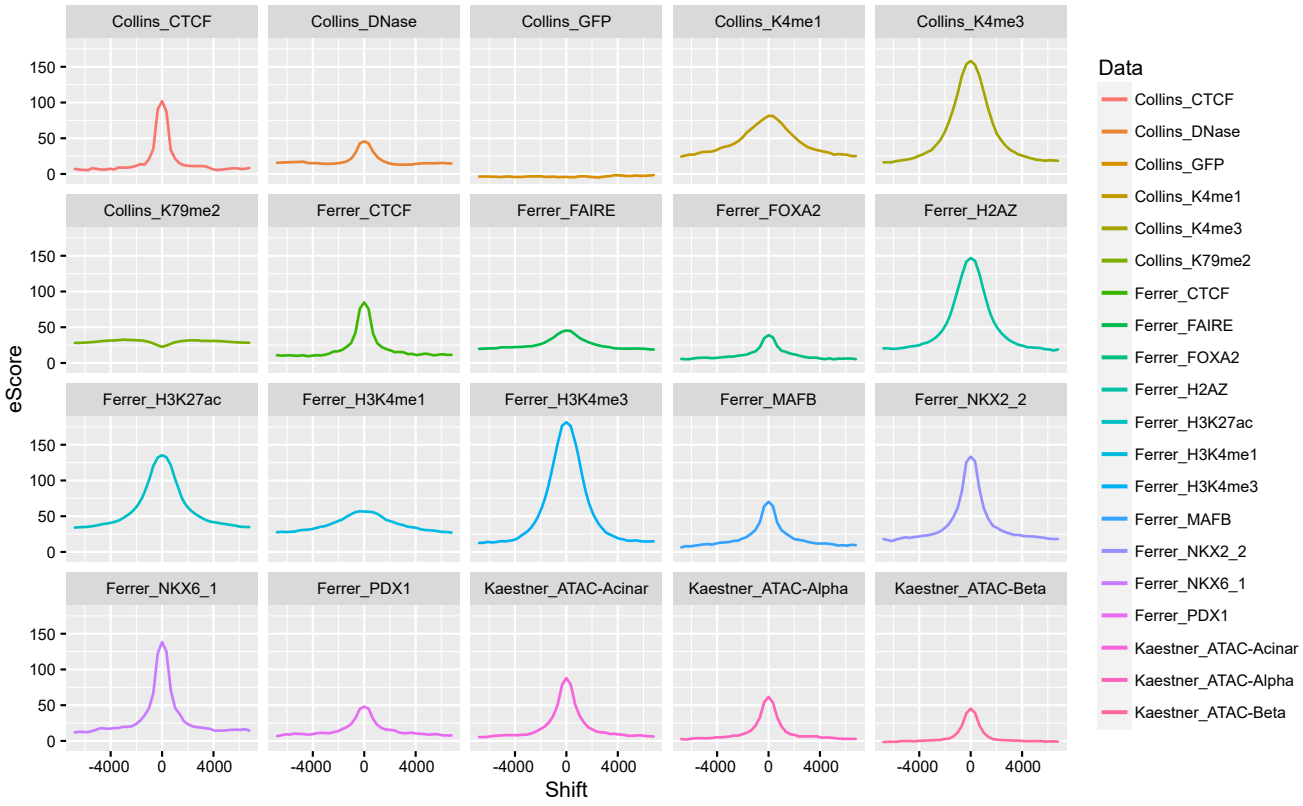

Figure S4. Enrichment scores between NFATC2 binding sites and histone marks, binding sites for other transcription factors, and chromatin architecture in human islets.
An enrichment score (eScore) evaluating the significance of the overlap of the NFATC2 peaks with various histone marks, transcription factors and chromatin accessibility measurements in human islets. All NFATC2 binding sites are centered at position zero while interrogating overlap between factors. The enrichment plots re-compute the test statistic after shifting the NFATC2 peaks by varying amounts. If the score attenuates as the shift increase, then the actual locations of the peaks is important for enrichment. All data shown is found to significantly co-occur with NFATC2 binding sites except Collins_GFP and Collins_K79me2.

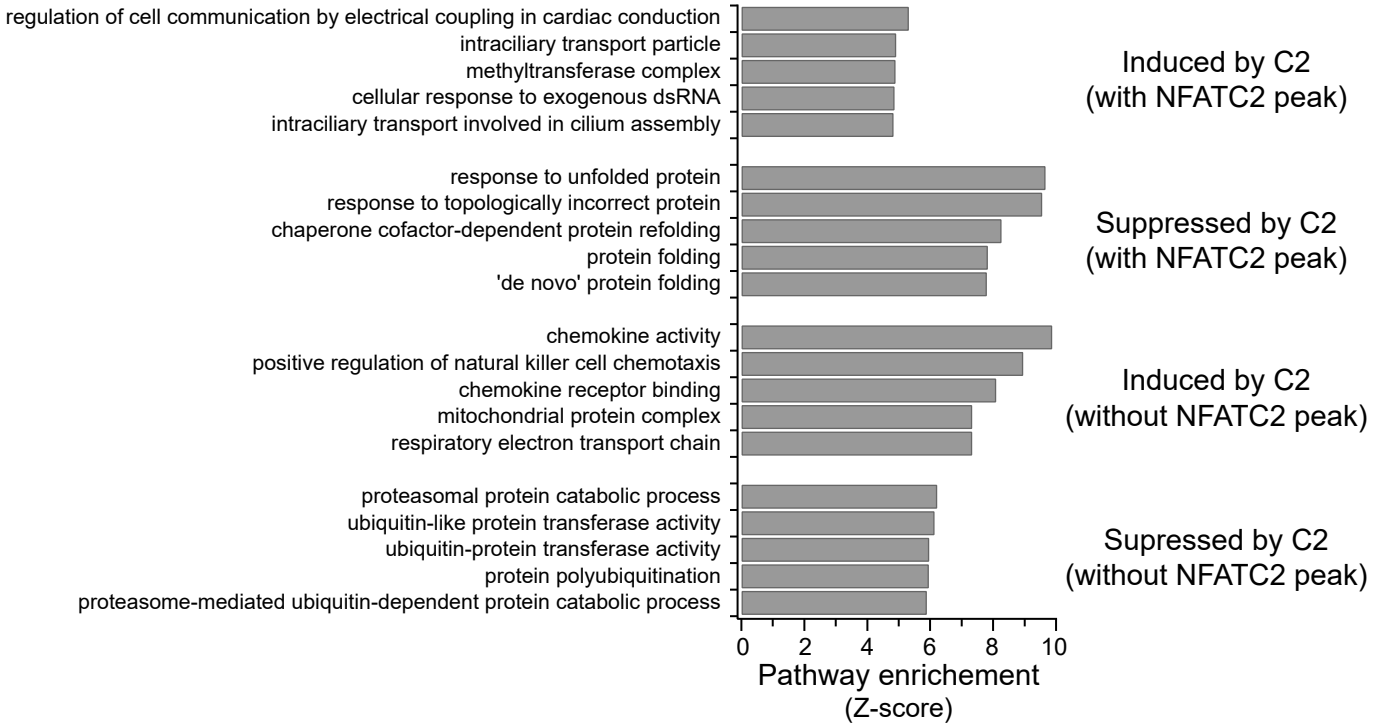

Figure S5. Gene set enrichment for NFATC2-regulated transcripts with a proximal NFATC2 binding site in human islets.

RNA-seq yielded ~4800 transcripts that were DE with NFATC2. To define direct targets of NFATC2 we sorted these DE genes by those that had an NFATC2 peak within 50 Kbp of its TSS and those that did not. These genes sets were further sorted by direction of expression change indicated to the right of the plot. Pathway enrichment using ALLEZ was performed on these gene sets and shown as a z-score. Only the top enriched terms are shown. All other terms can be found in Table S5.

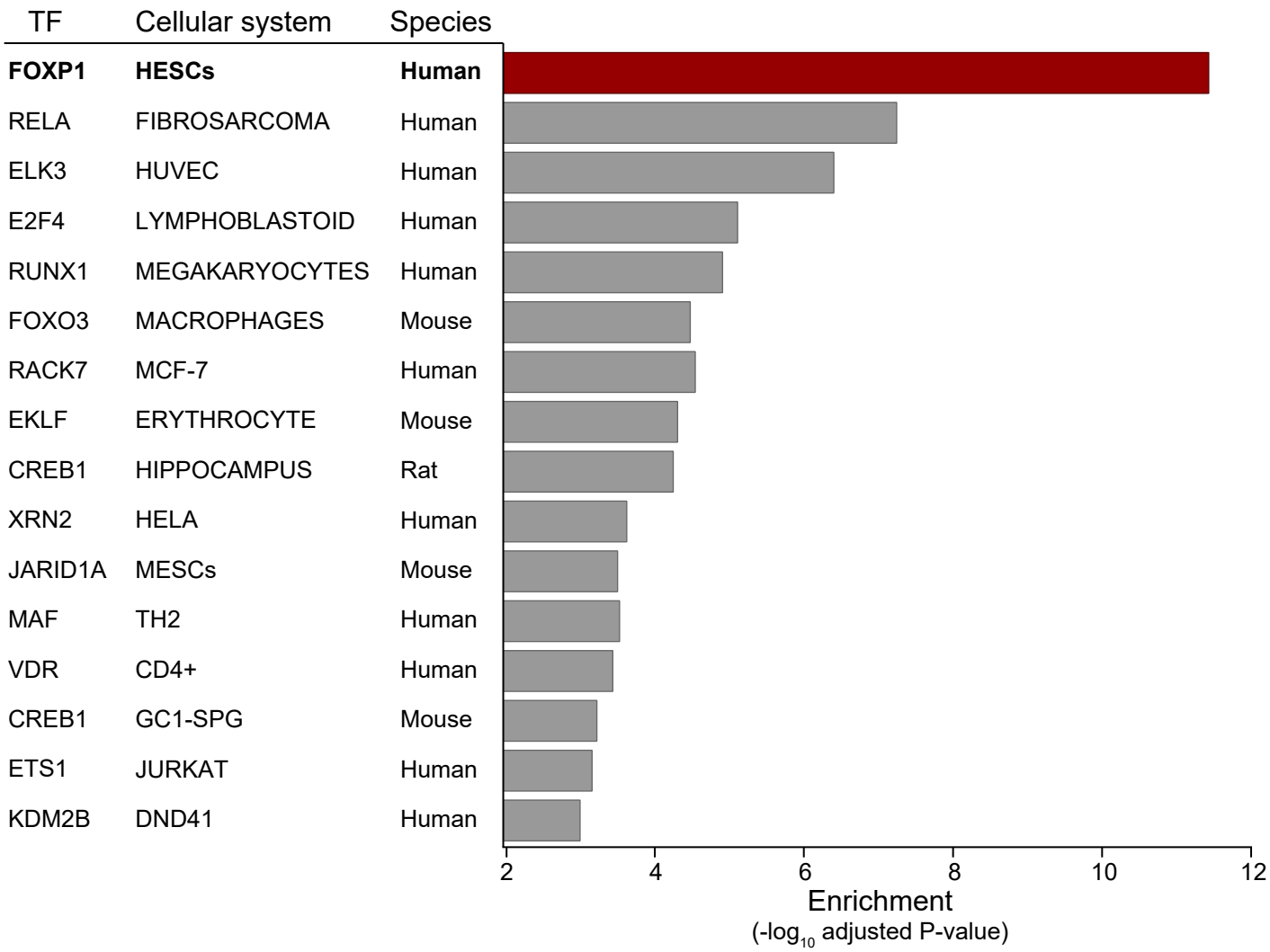

Figure S6. ChEA analysis for positively regulated NFATC2 direct targets.
A ChIP enrichment analysis was used to identify overlapping direct target genes of NFATC2 among a database of transcription factors (TF). To be considered a direct target, a ChIP peak for the indicated TF was found in the promoter of target gene. We selected 1425 genes that have increasing expression upon NFATC2 overexpression and have an NFATC2 ChIP peak within 50 Kbp. A Fisher's exact test was performed and the respective p-values of the top sixteen ChIP datasets with overlapping direct target genes are plotted. The most significantly enriched overlapping TF was FOXP1 in human embryonic stem cells.

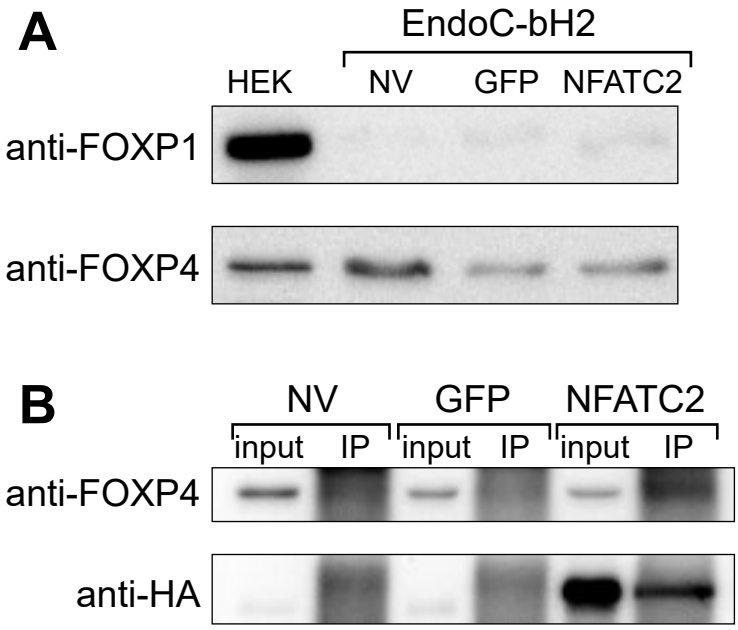

Figure S7. FOXP4 co-immunoprecipitates with NFATC2 in EndoC-βH2 human β-cells. A) Western-blot for FOXP1 and FOXP4 protein in HEK293 cells (HEK) and EndoC-βH2 β-cells without virus (NV), or with Ad-GFP (GFP) or Ad-ca-Nfatc2 (NFATC2). B) Immunoprecipation (IP) for the HA-tag on ca-Nfatc2 followed by Western blot for FOXP4 protein in EndoC-βH2 β-cells without virus (NV), or with Ad-GFP (GFP) or Ad-ca-Nfatc2 (NFATC2). A portion of each lysate sample (input) was saved for comparison to IP samples.

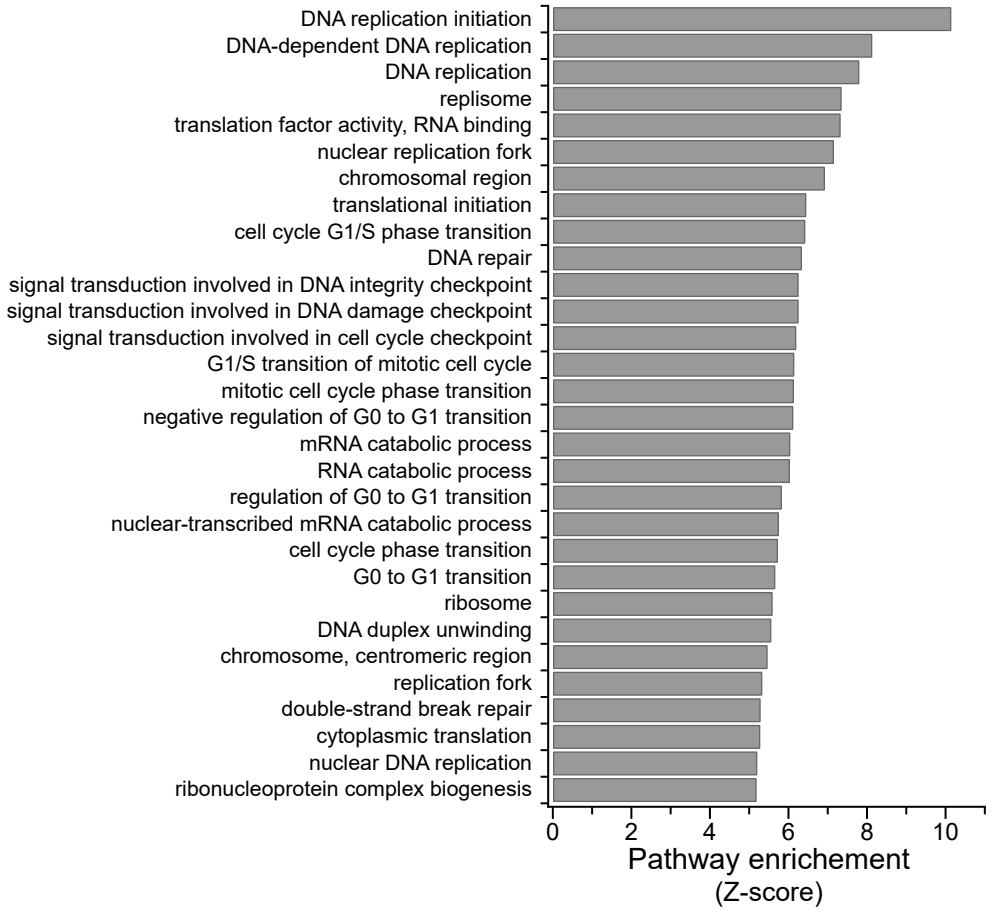

Figure S8. Gene set enrichment for NFATC1 and NFATC2-regulated transcripts that followed the β-cell proliferation signature in human islets.
NFATC2 direct targets that change expression in concordance with β-cell proliferation in human and mouse islets were subjected to pathway enrichment analysis using ALLEZ and shown as a z-score. These genes are plotted in Figure 4B.

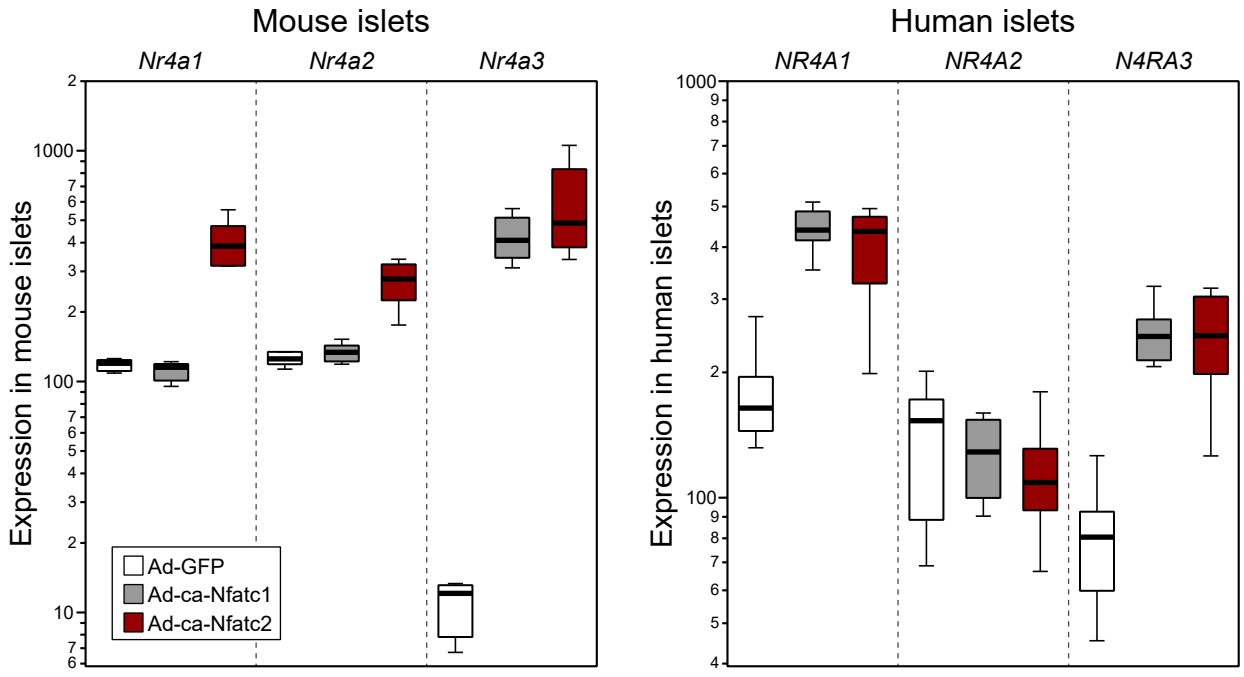

Figure S9. NFAT-dependent regulation of NR4A gene family in mouse and human islets. The expression of Nr4a1, Nr4a2, and Nr4a3 in human and mouse islets after treatment with Ad-GFP, Ad-ca-Nfatc1, or Ad-ca-Nfatc2 after 48 hours, measured in transcripts per million (TPM). N=5 for mouse islets. N=8 for human islets.

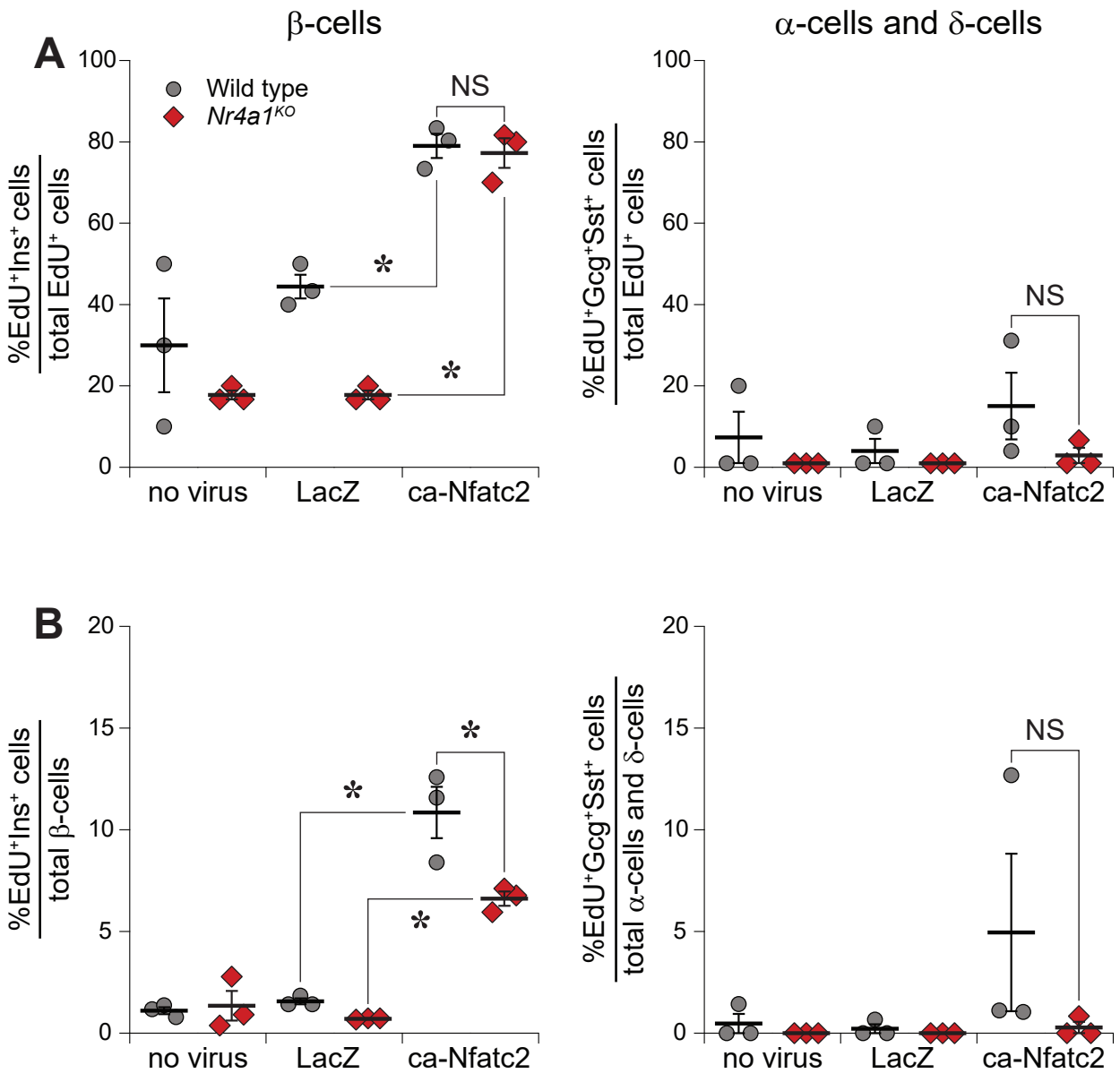

Figure S10. Effects of NFATC2 on β-cell proliferation, and the requirement of Nr4a1 for maximal stimulation.

Islets from wild type and *Nr4a1*^{KO} mice were treated with no virus, Ad-LacZ, or Ad-ca-Nfatc2, and incubated 48 hours with EdU to mark proliferating cells. Islets were dispersed to identify EdU+ cells, and co-stained with insulin, or glucagon and somatostatin to identify β-cells, or α-cells and δ-cells, respectively. A) Percentage of EdU+ β-cells (left panel) and α-cells/δ-cells (right panel) relative to all EdU+ cells. B) Percentage of EdU+ β-cells relative all β-cells (left panel) and EdU+ α-cells/δ-cells relative to all α-cells/δ-cells (right panel). Data represent mean ± SEM, * $P < 0.05$ for ca-Nfatc2 vs. LacZ, 2-way ANOVA, N=3 for each genotype.

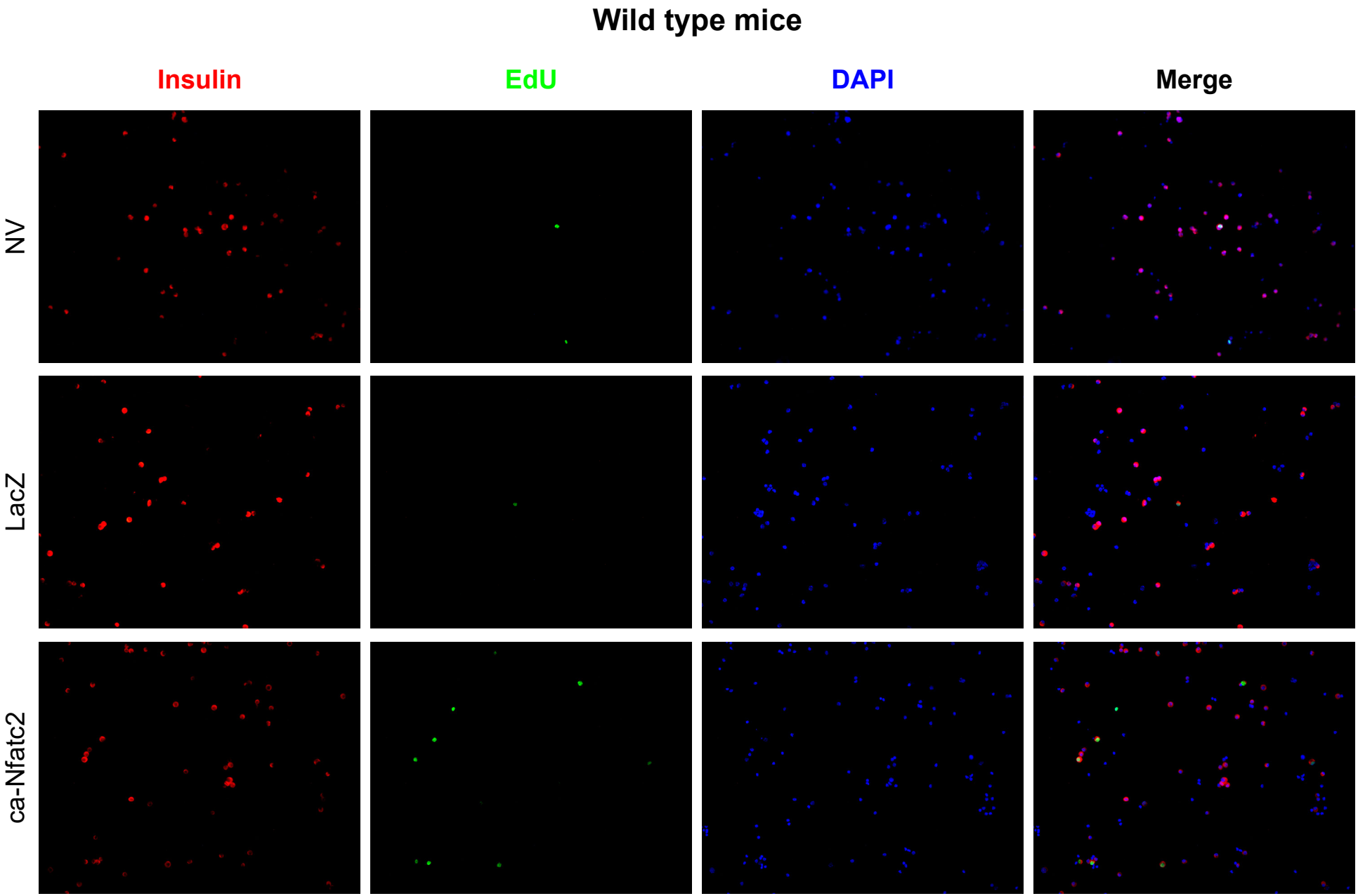

Figure S11. Representative images of dispersed wild type islets used to assess NFATC2-dependent β-cell proliferation. Dispersed islet cells were treated with no virus (NV) or with an adenovirus to overexpress LacZ or ca-Nfatc2, followed by immu-no-staining for EdU (green), DAPI (blue), or insulin (red).

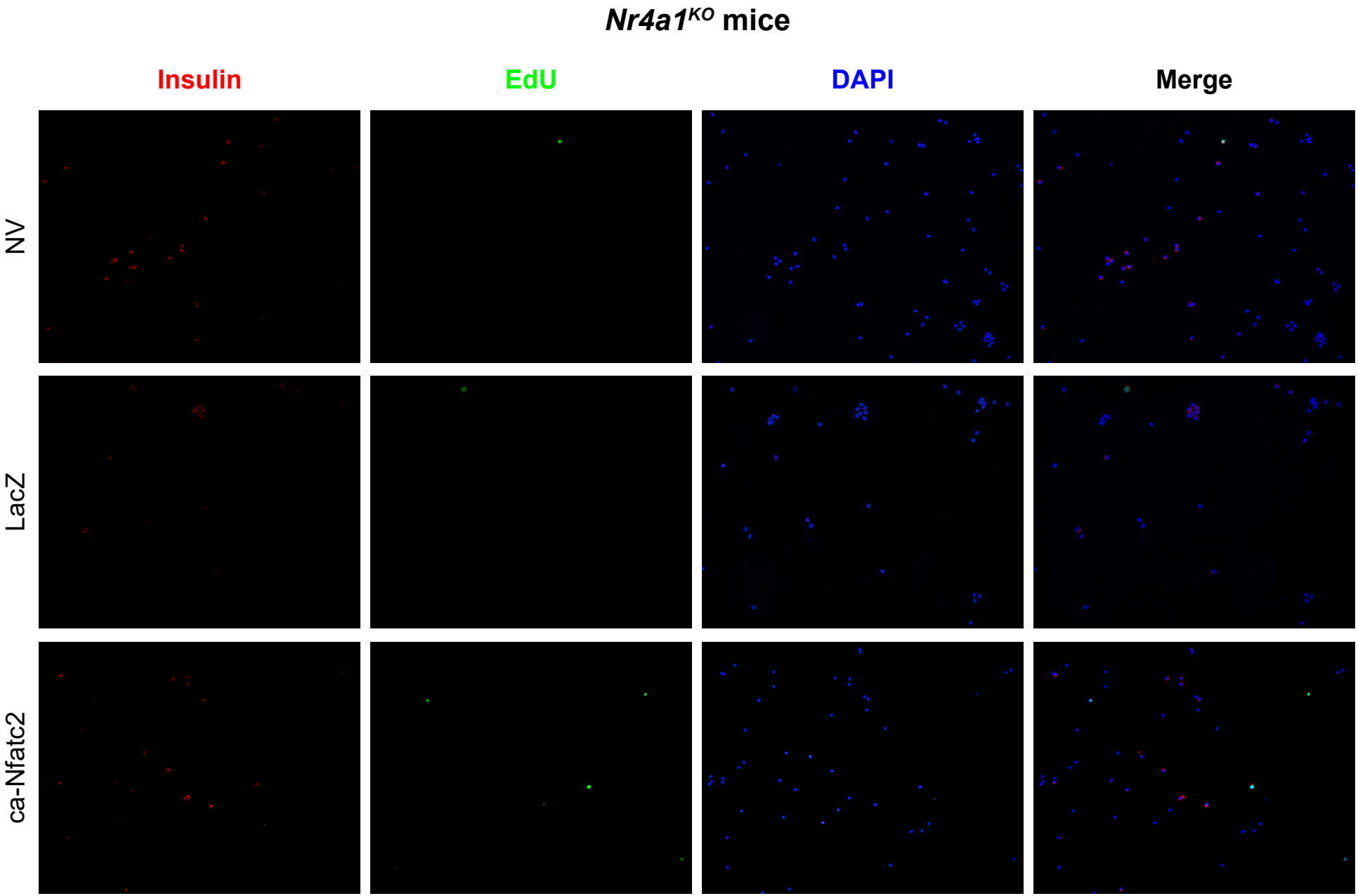

Figure S12. Representative images of dispersed *Nr4a1*^{KO} islets used to assess NFATC2-dependent β-cell proliferation. Dispersed islet cells were treated with no virus (NV) or with an adenovirus to overexpress LacZ or ca-Nfatc2, followed by immuno-staining for EdU (green), DAPI (blue), or insulin (red).

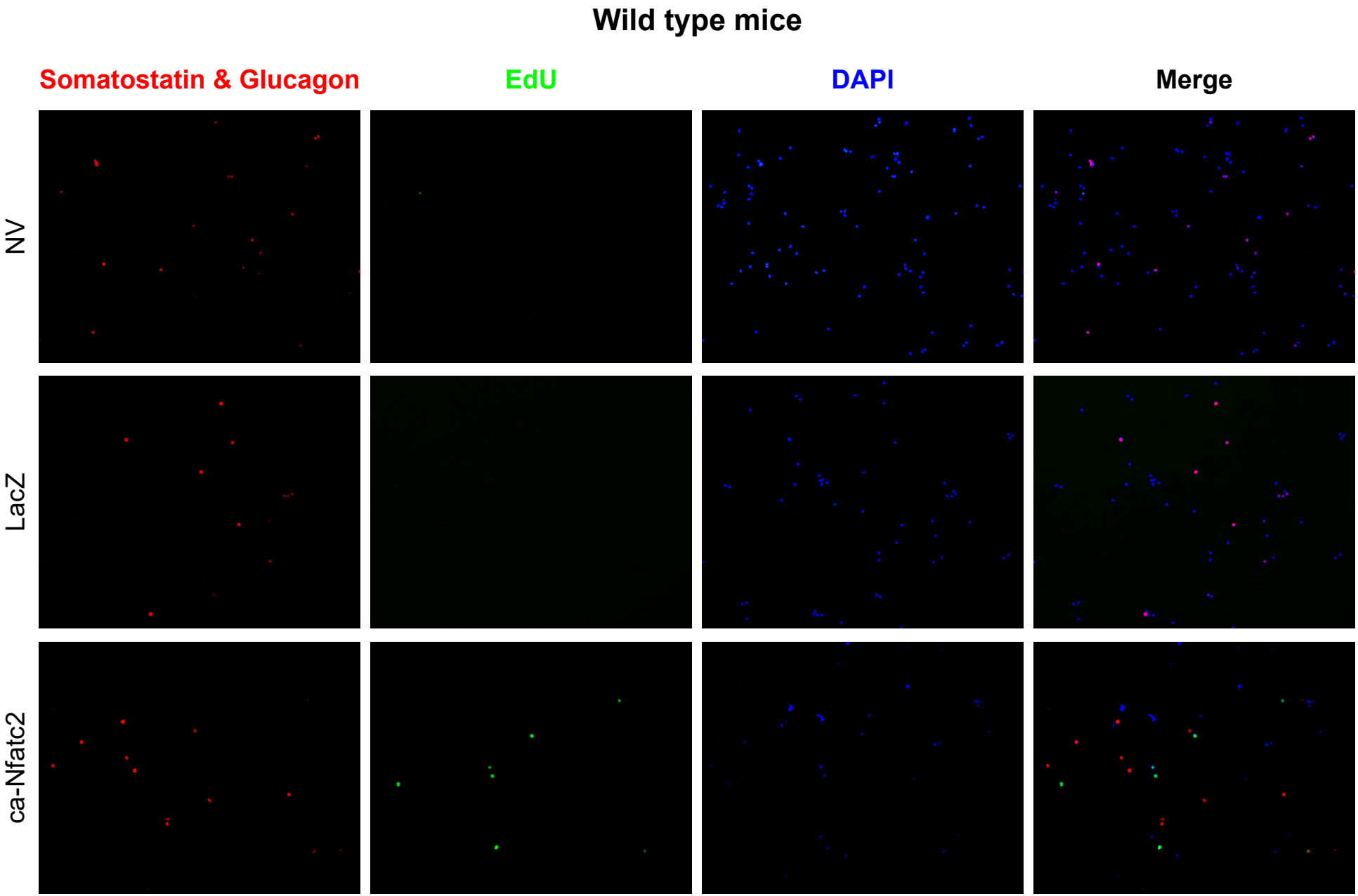

Figure S13. Representative images of dispersed wild type islets used to assess NFATC2-dependent α-cell and δ-cell proliferation.

Dispersed islet cells were treated with no virus (NV) or with an adenovirus to overexpress LacZ or ca-Nfatc2, followed by immu-no-staining for EdU (green), DAPI (blue), or glucagon and somatostatin (red).

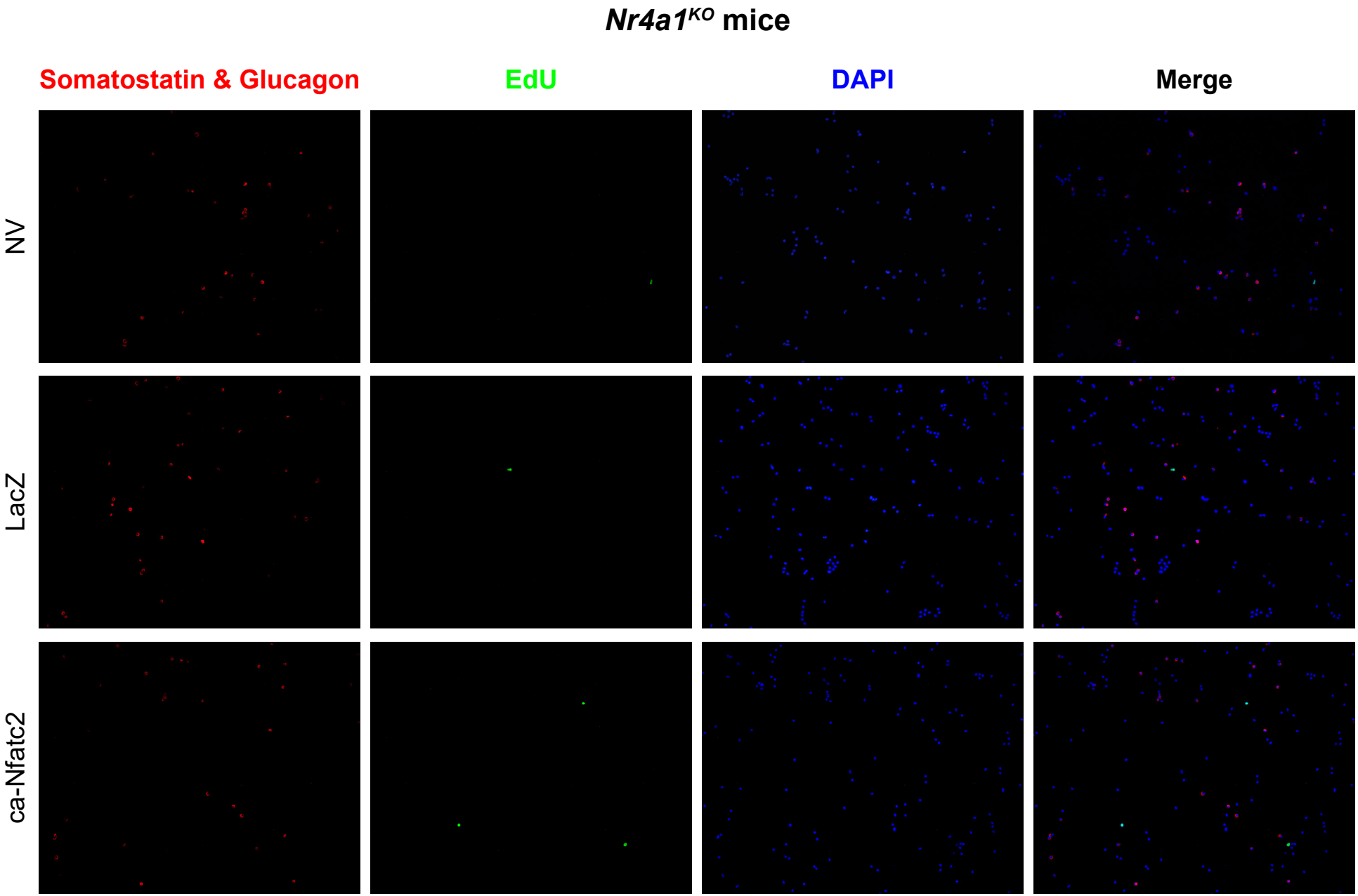

Figure S14. Representative images of dispersed *Nr4a1*^{KO} islets used to assess NFATC2-dependent α-cell and δ-cell proliferation.

Dispersed islet cells were treated with no virus (NV) or with an adenovirus to overexpress LacZ or ca-Nfatc2, followed by immu-no-staining for EdU (green), DAPI (blue), or glucagon and somatostatin (red).

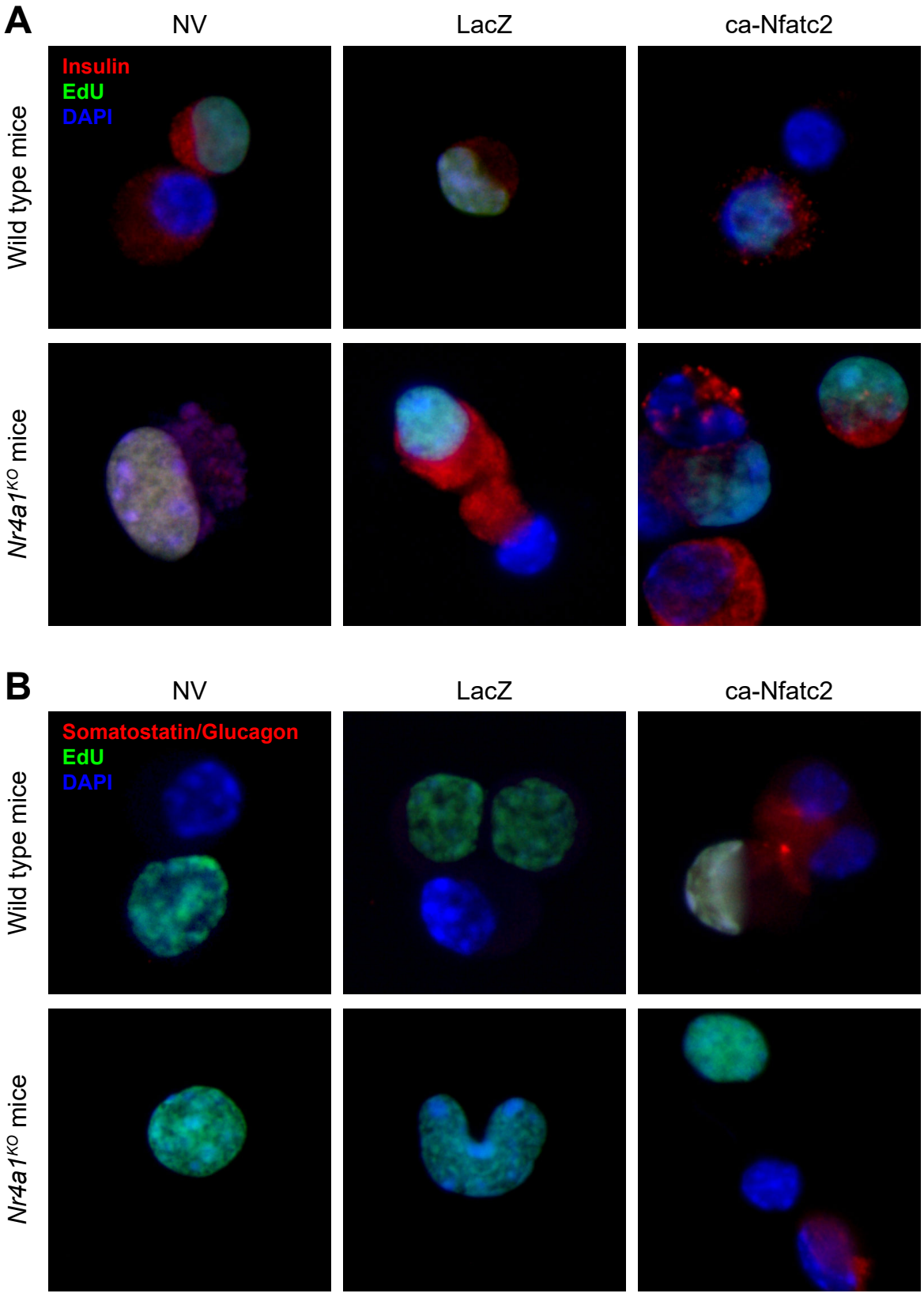

Figure S15. High-resolution images of proliferating islet cells from wild type and *Nr4a1*^{KO} mice.

Dispersed islet cells from wild type or *Nr4a1*^{KO} mice were treated with no virus (NV), or an adenovirus to overexpress LacZ or ca-Nfatc2, followed by immuno-staining for EdU, DAPI, or insulin (A), or glucagon and somatostatin (B).

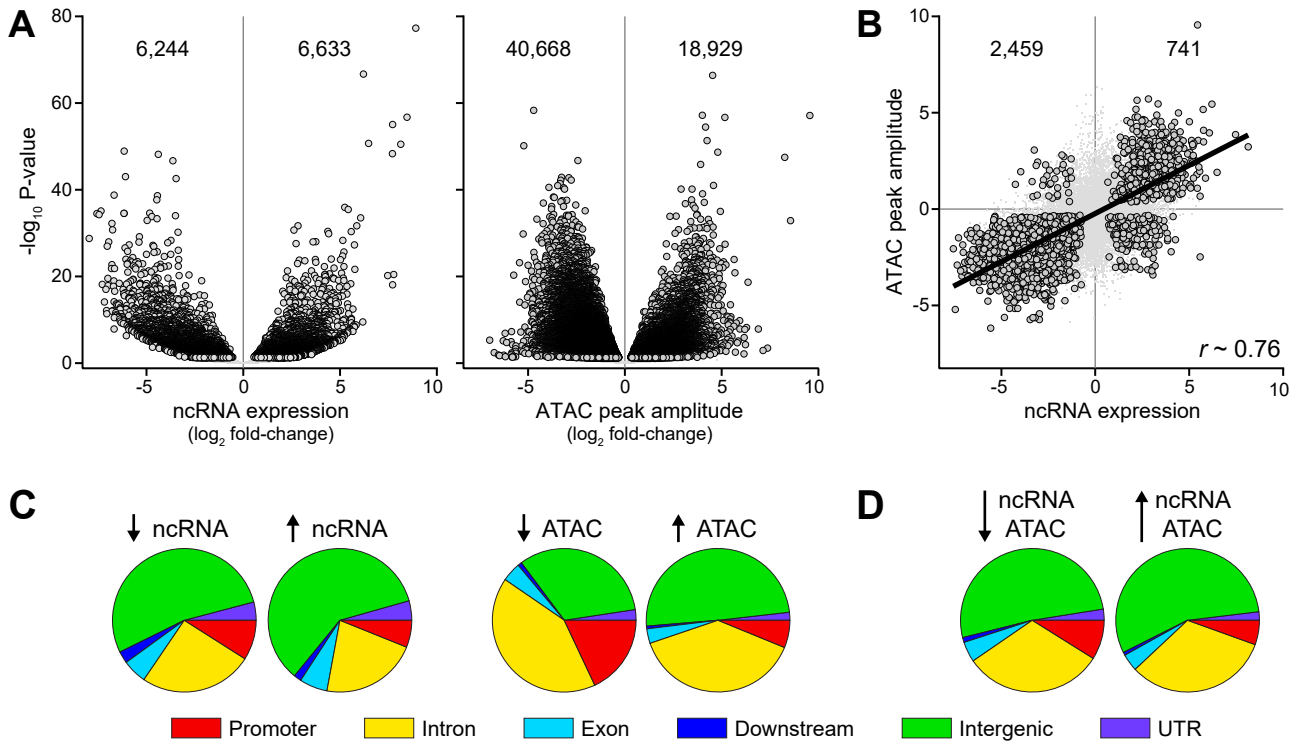

Figure S16. Global changes in ncRNA expression and chromatin accessibility induced by NFATC2 in human islets.

A) All differentially expressed ncRNAs and ATAC peaks quantified in human islets treated with Ad-GFP or Ad-ca-Nfatc2 are shown using -log10 p-value vs. log2 fold-change. B) All colocalized ncRNA and ATAC peaks found in human islets are plotted using the fold change in ATAC peak accessibility or ncRNA expression Ad-ca-Nfatc2/Ad-GFP. A Spearman correlation analysis suggests a positive correlation between ATAC peak opening and ncRNA expression (r ~0.76). A linear regression of significantly different ATAC peaks and ncRNAs was performed and the resulting line in plotted. C) The genomic compartment of all differentially expressed ncRNAs or ATAC peaks is shown as a pie chart, while discriminating between decreasing or increasing ncRNAs or ATAC peaks. D) The genomic compartment of all differentially expressed/accessible Colocalized ATAC-ncRNA pairs is shown as a pie chart, discriminating between concordantly decreasing or increasing pairs.

Full unedited gel images for Figure S7